Proceedings of the ASME 2021
International Mechanical Engineering Congress and Exposition
IMECE2021
November 1-5, 2021, Virtual, Online

IMECE2021-73012

THERMAL CIRCUIT ANALYSIS OF DROPLET EVAPORATION ON HOT MICROSTRUCTURED SUPERHYDROPHOBIC SURFACES

Wenge Huang
Department of Mechanical Engineering
Virginia Tech
Blacksburg, VA 24061

Xukun He
Department of Mechanical Engineering
Virginia Tech
Blacksburg, VA 24061

Jiangtao Cheng
Department of Mechanical Engineering
Virginia Tech
Blacksburg, VA 24061

ABSTRACT

In this paper, the evaporation dynamics of a water droplet dwelling on the hot micro-structured superhydrophobic surfaces was experimentally and theoretically investigated. For the first time, two distinguished components of mass/heat transfer, i.e., from droplet cap and base, during the droplet evaporation were systematically studied. Considering all the thermal resistances from the heated substrate to the droplet cap interface, a comprehensive thermal circuit model was developed to analyze the effect of micropillars and substrate temperature on the sessile droplet evaporation. As substrate temperature increases, a more apparent temperature mismatch between droplet cap and heated substrate was experimentally observed, which could be explained by increasing ratio of evaporation from the droplet base. Moreover, the increasing temperature of droplet cap during the evaporation could be successfully predicted by our model indicating the component of evaporative heat from droplet base (φ) is decreasing. This work could advance our understanding of droplet evaporation on heated superhydrophobic surfaces and further provide us a new tool to accurately predict droplet temperature and evaporation rate during the evaporation process.

Keywords: Evaporation, Thermal circuit model, Superhydrophobic surface

NOMENCLATURE

a	radius of micropillar
b	radius of water layer
D	diameter of the micropillar
D_d	diffusion coefficient
h	height of the water droplet
H	height of the micropillar
H_h	relative humidity
k	thermal conductivity
l	thickness
q	heat flux
R	thermal resistance
T	temperature
θ	contact angle
φ	evaporation ratio of the droplet base

1. INTRODUCTION

Droplet evaporation is a common phenomenon in nature and has been applied in various applications including ink-jet printing [1], spray cooling [2] and micro fabrication [3]. The droplet evaporation on hydrophobic surface is quite different from the evaporation on hydrophilic surfaces due to the decrease of wettability. In the past two decades, inspired by nature structures such as lotus leaf, "superhydrophobic" surfaces with micro or nanoscale roughness were invented to exhibit larger hydrophobicity. Generally, there are two kinds of wettings states for droplet on the micro-structured substrates [4]: (a) Cassie state: the droplet only touches the top surface of the microstructures and leaves air cavities underneath the droplet; and (b) Wenzel state: droplet completely penetrate the cavity between micropillars. It has been found the distinct pinning/depinning mechanism in these two wetting states would lead to completely different heat and mass transfer dynamics during sessile droplet evaporation on superhydrophobic surfaces [5] [6].

For the evaporation of droplets in Wenzel state on superhydrophobic, only the heat and mass transfer at the liquid-vapor interface of droplet cap should be considered which is similar with the sessile droplet evaporation on smooth surface [7-9]. However, for the sessile droplet evaporation in Cassie state, two different components of the evaporation occur at the liquid-vapor interface *i.e.,* the droplet cap surface and droplet base surface should be taken into consideration. if the sessile droplet is evaporated at room temperature or on heated substrates with a relatively low temperature, the evaporation from the droplet base is always neglected because of the small surface area and large pressure resistance between the micropillars. In a previous study, a diffusion-driven model only considering the evaporation at the droplet cap surface was reported which could successfully predict the evaporation dynamics of sessile droplet

at room temperature on micropillar surface [10]. As the substrate temperature increases, the mass and heat flux across the droplet base will be significantly increased thus could not be neglected anymore [11-13]. Nevertheless, the effect of larger heat flux from droplet base on droplet evaporation in Cassie state has been limited studied.

In this study, the evaporation dynamic of water droplet on heated superhydrophobic microstructured substrates will be experimentally and theoretically investigated. Based on a comprehensive thermal resistance analysis, a thermal circuit model would be developed to predict the droplet cap surface temperature. Furthermore, the evolution of evaporation ratio of the droplet base during drop evaporation on heated superhydrophobic surface from 40 °C to 100 °C will be explored.

2. MATERIALS AND METHODS.

2.1 Substrates fabrication

Silicon-based microstructured substrates in this work are fabricated by the standard photolithography process and deep reactive ion etching (DRIE). The microstructure of substrates was characterized by the scanning electron microscope (SEM) as shown in Fig. 1. The diameter (D), height (H) and periodicity (P) of the micropillar used in this study are 20 μm, 40 μm and 40 μm, respectively.

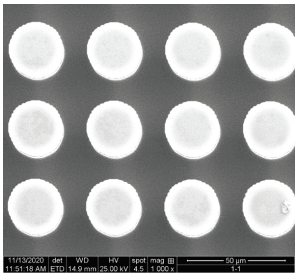

FIGURE 1: SEM IMAGE OF S1 SAMPLE

Subsequently, all the substrates were conformally coated with silane (Trichloro (1H,1H,2H,2H-per fluoroethyl)-silane, Sigma-Aldrich) using standard chemical vapor deposition (CVD) process[14] . Then the substrates were baked in 90°C for 60 min to generate the superhydrophobicity. And the static contact angle of water droplet on all the substrates is ~155° . To mitigate the sample edges effect on the droplet evaporation process, samples were cut into square pieces with 2 cm length of side and water droplets were deposited at the center of the substrates.

2.2 Experiment setup

The experiment setup of this study is shown in Fig. 2. 4μL droplets were placed on the superhydrophobic substrate for evaporation. Substrate was heated by hot plate from 40 °C to 100 °C. The surface temperature of the hot plate was measured by thermocouple. An infrared (IR) camera was used to measure the surface temperature of the droplet and a high-speed camera was used to record the sessile droplet evaporation from side-view in a frame rate of 1.14 frame /s. And the contact angle, contact radius and height of evaporating droplet were obtained by analyzing the transient images.

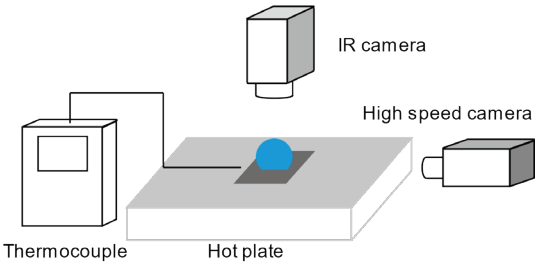

FIGURE 2: EXPERIMENTAL SETUP INCLUDING HOT PLATE, HIGH SPEED CAMERA, IR CAMERA AND THERMOCOUPLE

2.3 Theoretical model

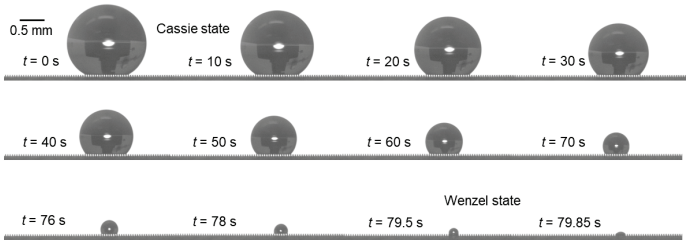

FIGURE 3: SNAPSHOTS OF DROPLET EVAPORATION ON SUPERHYDROPHOBIC SURFACE.

When placed on the superhydrophobic surfaces, the initial sessile droplet in Cassie state would only touch the top surface of the micropillars, which could be evidenced by air cavities observed underneath the water droplet shown in Fig. 3. During majority time of the evaporation, the droplet would stay in Cassie state and only transit to wetting state at the very end of the evaporation.

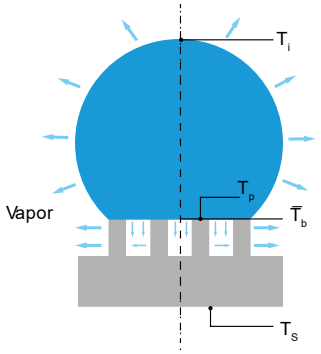

FIGURE 4: DIAGRAM OF DROPLET EVAPORATION ON SUBSTRATE SURFACE.

During the evaporation of sessile droplet in Cassie state on micropillared surface, an energy balance could be derived:

$$q_s = q_{temp} + q_{conv} + q_{rad} + q_{evap} \quad (1)$$

where q_s the total energy transferred from the substrate to droplet; q_{temp} is the energy required for the water temperature increase; q_{conv} is the convective heat transfer from the water droplet to the ambient air; q_{rad} is the radiation heat transfer from water droplet to the ambient air; q_{evap} is the heat released to the ambient air through evaporation.

$$q_{temp} = c_p \rho_w V \frac{dT_w}{dt} \quad (2)$$

$$q_{rad} = \varepsilon \sigma S (T_w^4 - T_\infty^4) \quad (3)$$

$$q_{conv} = h_{conv} S (T_w - T_\infty) \quad (4)$$

$$q_{evap} = h_{fg} \rho_w \frac{dV}{dt} \quad (5)$$

where c_p, ρ_w, T_w V and h_{fg} are the specific heat capacity, density, temperature, volume and latent heat of the droplet water respectively; ε is the emissivity of the water droplet interface and σ is the Boltzmann constant; S is the liquid-vapor interface area and h_{conv} is the natural convection heat transfer coefficient of the ambient air.

At a relatively higher temperature (T > 40°C), evaporation-induced heat transfer q_{evap} should be dominant over the other three types of heat transfer [5]. Thus, the overall heat transfer from the substrate to the water droplet could be estimated as the heat released from droplet to the ambient air through evaporation.

$$q_s = q_{evap} \quad (6)$$

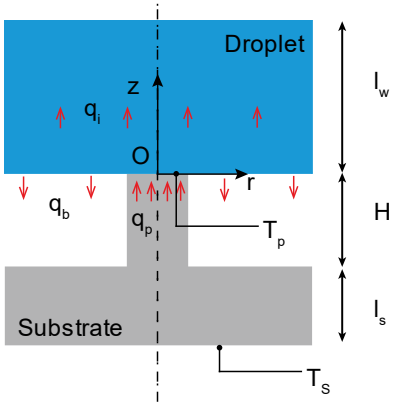

FIGURE 5: DIAGRAM OF HEAT TRANSFER PROCESS FROM MICROPILLAR TO WATER DROPLET

In general, both the heat transfers from the substrate to the micropillars and the vapor cavities should be considered. However, the thermal resistance of the vapor is much larger than that of the silicon pillars due to the significant ratio between the thermal conductivity of silicon pillars (100 $Wm^{-1}K^{-1}$) [15] [16] and water vapor (0.025 $Wm^{-1}K^{-1}$) [17]. Therefore, it is reasonable to assume the heat primarily conducts from the pillar to the water droplet whereas the vapor-solid interface of cavities boundary can be regarded as adiabatic.

Considering the periodicity of the pillar arrays, we can focus on one unit cell of the pillar array consisting of one pillar and one vapor cavity as shown in Fig. 5. As we mention before, heat transferred from the substrate is equal to that released to the ambient air. Thus, we can calculate the substrate heat flux by obtaining the evaporation flux of the water droplet based on the decreasing droplet volume (Eq. 5). We assume the heat flux is uniform from the substrate. Thus, heat flux across one unit cell could be calculated as:

$$q_p = \frac{q_s}{N} \quad (7)$$

where N is the number of the micropillar underneath the droplet.

The thermal resistance of the silicon substrate per unit cell could be calculated as:

$$R_s = \frac{l_s}{k_{Si} P^2} + \frac{4H}{k_{Si} \pi D^2} \quad (8)$$

where k_{Si} is the thermal conductivity of silicon and l_s is the thickness of the silicon substrate excluding the height of pillars,

Based on the energy balance inside the silicon substrate, the temperature on the top surface of the micropillar could be calculated as:

$$T_p = T_s - \frac{q_p}{R_s} \quad (9)$$

To study the temperature distribution near the liquid-solid interface, i.e., the top surface of micropillar inside the water droplet, a thin water layer with a thickness of l_w in a unit cell (Fig. 5) would be considered. The conductive heat transfer equation in this water layer is:

$$\frac{\partial^2 T}{\partial r^2} + \frac{1}{r}\frac{\partial T}{\partial r} + \frac{\partial^2 T}{\partial z^2} = 0 \quad (10)$$

Due to the small size of the micropillar, the heat flux across the liquid-solid interface and liquid-vapor interface in a unit cell could be assumed as uniform. As a result, we have the first boundary condition:

$$k_w \frac{\partial T}{\partial z} = \begin{cases} \frac{q_p}{\pi a^2} & 0 < r < a; \quad z = 0 \\ -\frac{q_b}{\pi (b^2 - a^2)} & a < r < b; \quad z = 0 \end{cases} \quad (11)$$

where k_w is the thermal conductivity of water, a is the radius of the micropillar and b is the radius of the water cylinder in one unit cell.

On the other side, the surface area of droplet base is significantly larger than the top area of micropillars. Hence, a constant temperature boundary could be assumed at $z = l_w$:

$$T(r; z) = T_w \qquad 0 < r < b; \quad z = l_w \quad (12)$$

Moreover, considering the periodicity of the unit cell, we can assume it is adiabatic between unit cell with its neighbor cell in water layer. Thus, we obtain the adiabatic boundary condition:

$$\frac{\partial T}{\partial r} = 0 \qquad r = b; \quad 0 < z < l_w \quad (13)$$

Solving the heat transfer equation Eq. (10) with the three boundary conditions Eq. (11), Eq. (12), Eq. (13), we can obtain the temperature distribution inside the water layer as:

$$T_b = T_w + \frac{q_p (l_w - z)}{k_w} \left(\frac{a^2}{b^2} (1 + \varphi) - \varphi \right) + \frac{2 a q_p (1+\varphi)}{k_w l_w} \sum_{n=1}^{\infty} \left[J_1 \left(\frac{a}{b} \alpha_n \right) J_0 \left(\frac{r}{b} \alpha_n \right) / \left(\alpha_n^2 J_0^2 (\alpha_n) \right) \right] \frac{sinh\left(\frac{\alpha_n}{b} (l_w - z) \right)}{cosh\left(\frac{\alpha_n}{b} l_w \right)} \quad (14)$$

where φ is the evaporation ratio , which is defined as the heat transfer across droplet base over overall heat transfer from substrate to droplet: $\varphi = q_b / q_p$. $J_0(x)$ and $J_1(x)$ are the first kind Bessel functions with order of 0 and 1, respectively, α_n is the n-th root of $J_1(x)$=0.

The temperature at the droplet base at z=0 is calculated as:

$$T_b = T_w + \frac{q_p l_w}{k_w}\left\{\frac{a^2}{b^2}(1+\varphi) - \varphi + \frac{2a(1+\varphi)}{l_w}\sum_{n=1}^{\infty}\left[J_1\left(\frac{a}{b}\alpha_n\right)J_0\left(\frac{r}{b}\alpha_n\right)/\left(\alpha_n^2 J_0^2(\alpha_n)\right)\right] tanh\left(\frac{\alpha_n}{b}l_w\right)\right\} \quad (15)$$

Thus, the average temperature of the droplet base could be obtained as:

$$\bar{T}_b = \frac{\int_0^b 2\pi r T_b(r)dr}{\pi b^2} \quad (16a)$$

$$\bar{T}_b = T_w + \frac{q_p l_w}{k_w}\left\{\frac{a^2}{b^2}(1+\varphi) - \varphi\right\} \quad (16b)$$

The average temperature of the solid-liquid interface at droplet base could be estimated as:

$$T_{b,p} = \frac{\int_0^a 2\pi r T_b(r)dr}{\pi a^2} \quad (17a)$$

$$T_{b,p} = \bar{T}_b + \left\{\frac{q_p 2a(1+\varphi)}{k_w}\sum_{n=1}^{\infty}\left[J_1^2\left(\frac{a}{b}\alpha_n\right)/\left(\alpha_n^3 J_0^2(\alpha_n)\right)\right] tanh\left(\frac{\alpha_n}{b}l_w\right)\right\} \quad (17b)$$

Due to temperature continuity at the solid-liquid interface, we should have:

$$T_{b,p} = T_p \quad (18)$$

Thus, the base average temperature of the water droplet could be obtained as:

$$\bar{T}_b = T_p - \frac{q_p 2a(1+k)}{k_w}\sum_{n=1}^{\infty}\left[J_1^2\left(\frac{a}{b}\alpha_n\right)/\left(\alpha_n^3 J_0^2(\alpha_n)\right)\right] \quad (19)$$

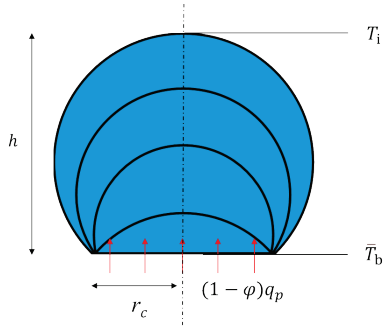

FIGURE 6: DIAGRAM OF HEAT TRANSFER THROUGH WATER DROPLET

Considering the heat balance inside the droplet, the shape of sessile droplet should be assumed to spherical cap. Thus, the thermal resistance of the water droplet could be estimated as: [18] [19]

$$R_w = \frac{arctan\left(\frac{h}{r_c}\right)}{2\pi k_w r_c} \quad (20)$$

where h is the height of the water droplet, r_c is the contact radius of the water droplet.

Thus, the temperature at the cap of the water droplet could be estimated as:

$$T_i = \bar{T}_b - (1-\varphi)q_p R_w \quad (21)$$

With the water droplet interface temperature, we can calculate the evaporation rate from the droplet cap surface based on the diffusion-driven model:

$$q_e = \frac{\pi r_c D_d (c_s - H_h c_\infty) f(\theta)}{h_{fg}} \quad (22)$$

where D_d is the coefficient of vapor diffusion, c_s is the saturated vapor concentration of the droplet surface, c_∞ is the saturated vapor concentration of the environment, H_h is the relative humidity and $f(\theta)$ is a function of the droplet contact angle:

$$f(\theta) = \frac{sin(\theta)}{1+cos(\theta)} + 4\int_0^\infty \frac{1+cosh(2\theta\tau)}{sinh(2\pi\tau)} tanh\left[(\pi-\theta)\tau\right] d\tau \quad (23)$$

Since the energy for the evaporation is transferred from the substrate, the evaporation flux from the droplet cap should be the same as the heat flux transferred through the water droplet. Thus, we have the relation:

$$q_e = (1-\varphi)q_p \quad (24)$$

Solving Eq. (24), we can obtain the droplet interface temperature T_i and the evaporation ratio from the droplet base φ.

3. RESULTS AND DISCUSSION

In this study, we analyzed the evaporation process of small water droplet with 4 μL. The evolution of water droplet volume with respect to evaporation time is shown in Fig. 7. With the increase of the substrate temperature, the total evaporation time decreased. Moreover, the evaporation time t_e can be fitted with a power law function as the substrate temperature T_s, *i.e.*, $t_e = mT_s^n$, where $m = 1028380$ and $n = -2.01$.

The evolution of evaporation rate of water droplet heated at different temperature during the evaporation is shown in Fig. 8. here, the nondimensional time could be defined as the ratio of evaporation time and the total evaporation time. With the increase of the substrate temperature, the evaporation rate of water droplet is significantly increased, which could be simply attributed to the higher surface temperature of the water droplet. However, as droplet evaporates, its evaporation rate would gradually decrease, which could be explained by the decrease of the liquid-vapor interface of the water droplet during the evaporation.

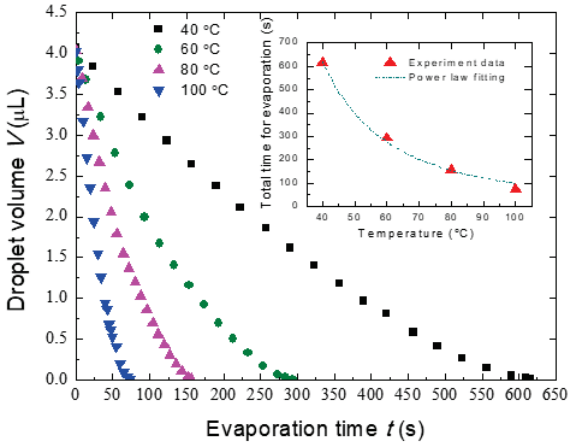

FIGURE 7: VARIATION OF DROPLET VOLUME AND TOTAL EVAPORATION TIME

The variation of droplet contact angle and nondimensional contact radius with respect to nondimensional time is shown in Fig. 9. At the beginning of evaporation, it is observed that the

contact angle continuously decreases and the nondimensional contact radius keeps unchanged. which could be characterized as constant contact radius (CCR) mode. After $\tau = 0.65$, the contact angle keeps constant at around 115° and the nondimensional contact radius starts to decrease. In this time period of $\tau = 0.65 \sim 0.9$, droplet evaporates in a constant contact angle (CCA) mode. Before the end of evaporation, both the contact angle and the nondimensional contact radius would decrease abruptly in a very short time, which is generally regarded as mixed mode.

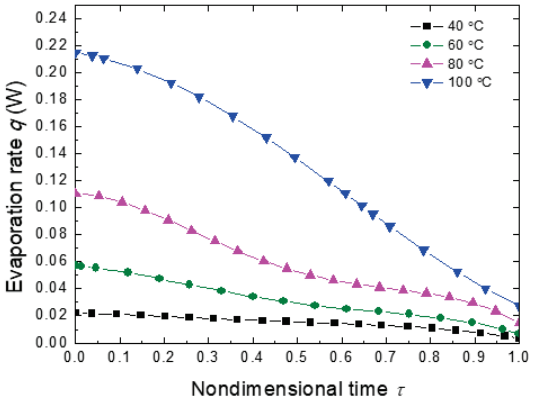

FIGURE 8: VARIATION OF DROPLET EVAPORATION RATE WITH TIME.

Based on the measured evaporation rate and developed thermal circuit model, instantaneous temperature of droplet interface during the evaporation could be calculated for different substrate temperature as illustrated in Fig. 10. Droplet surface temperature measured by the IR camera is also shown in Fig. 10. It can be observed from both the experimental value and model predicted value of droplet temperature increase as droplet evaporates. An apparent temperature mismatch between the droplet surface and substrate could be observed, which should be induced by the evaporative cooling. However, as substrate temperature increases, this mismatch is found to be enhanced from 7℃ to 25℃, which could be ascribed to the significant larger ratio of evaporation across the droplet base. The validity of our model could also be verified by the good agreement between the experimental measured value and model predicted value of droplet cap temperature.

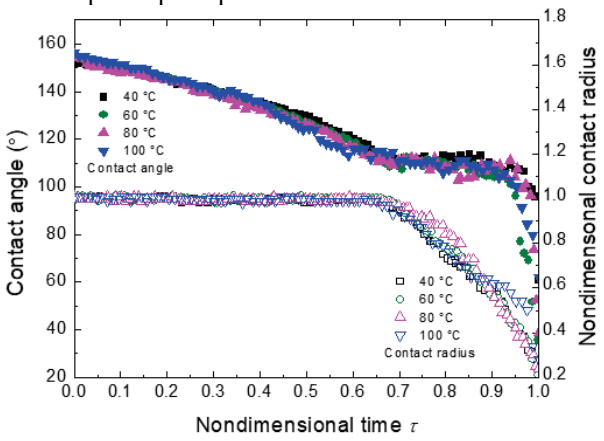

FIGURE 9: VARIATION OF DROPLET CONTACT ANGLE AND NONDIMENSIONAL CONTACT RADIUS

The evolution of evaporation ratio φ of an evaporating droplet on a substrate with different temperatures is shown in Fig. 11. As substrate temperature increases, the evaporation ratio φ increases, which means the larger portion of evaporation heat dissipation would occur at the droplet base. For certain cases, the evaporation ratio of the droplet base keeps on decreasing during the whole evaporation process which may be induced by the increase of the droplet cap temperature.

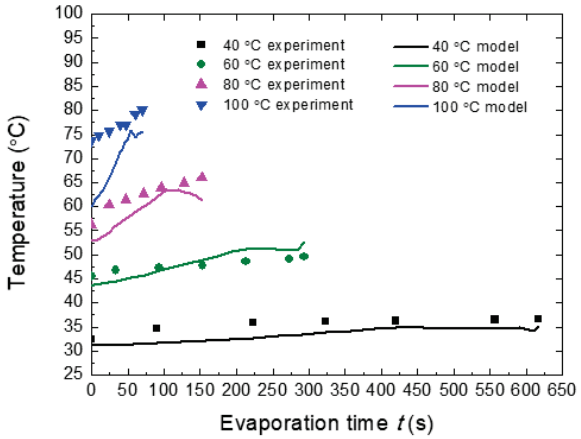

FIGURE 10: EVOLUTION OF DROPLET SURFACE TEMPERATURE.

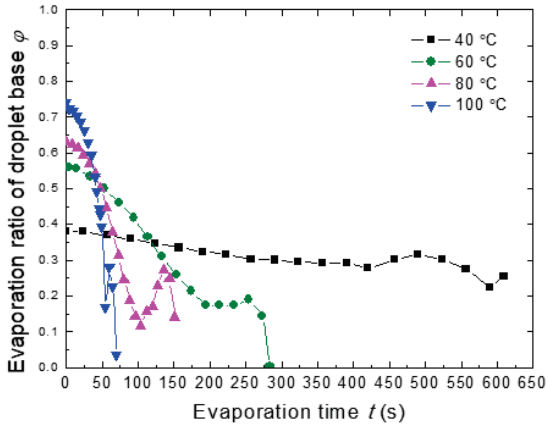

FIGURE 11: EVAPORATION RATIO FROM THE DROPLET BASE.

4. CONCLUSION

In this work, the water droplets evaporation on heated superhydrophobic surfaces is experimentally and theoretically investigated. We developed a thermal circuit model to analyze the evaporation dynamics, calculated the droplet surface temperature and the ratio of evaporation across the droplet base. The larger extent of temperature mismatch between droplet cap and substrate was firstly explained by the increasing ratio of evaporation from the droplet base as substrate temperature increases.

ACKNOWLEDGEMENTS

This work is financially supported by NSF CBET under grant number 1550299 and NSF ECCS under grant number 1808931.

REFERENCES

[1] P. Calvert. *Chem. Mater*, 2001

[2] W. Jia, H.H. Qiu. *Exp. Therm. Fluid Sci*, 2003

[3] D. Xia, S.R.J. Brueck. *Nano Lett*, 2008

[4] A. Cassie, S. Baxter. *Trans. Faraday Soc,* 1944

[5] R. Hays, D. Maynes, J. Crockett. *Int. J. Heat Mass Transfer,* 2016

[6] K. Sefiane, R. Bennacer. *J. Fluid Mech*, 2011

[7] T. A. H. Nguyen, S. R. Biggs, A. V. Nguyen. *Langmuir,* 2018

[8] Y. O. Popov. *Phys. Rev. E*, 2000

[9] S. Dash, S. V. Garimella. *Phys. Rev. E*, 2014

[10] G. McHale, S. Aqil, N. J. Shirtcliffe, M. I. Newton, H. Y. Erbil. *Langmuir,* 2005

[11] S. Adera, R. Raj, R. Enright, E. N. Wang. *Nat. Commun*, 2013

[12] M. Wei, Y. Song, Y. Zhu, D. Preston, C. S. Tan, E. N. Wang. *Appl. Phys. Lett*, 20202

[13] H. Kim, B. Truong, J. Buongiorno, L. Hu. *Appl. Phys. Lett*, 2011

[14] M. Badv, I. H. Jaffer, J. I. Weitz, T. F. Didar. *Sci. Rep*, 2017

[15] P. Maycock. *Solid-state Electron*, 1967

[16] C. Glassbrenner, G. A. Slack. *Phys. Rev.* 1964

[17] A. L. Biance, C. Clanet, D. Quere. *Phys. Fluids*, 2003

[18] S. Kim, K. Kim. *J. Heat Transfer*. 2011

[19] N. Miljkovic R. Enright. E. N. Wang. *ACS Nano*, 2012